Assessment of Potential Impact of Stratospheric Flight on Earth's Ultraviolet Irradiance

Henry Hidalgo
Institute for Defense Analyses, Arlington, Va.

Introduction

THIS paper is a partial summary of theoretical work described in monographs 3 and 4 (in press) of the Climatic Impact Assessment Program (CIAP) of the U.S. Department of Transportation.[1,2] The scope of the paper is limited to a description of the methodology for assessing the potential increase in solar ultraviolet (UV) radiation at the earth's surface from stratospheric flight. Such UV radiation increase would be a consequence of the atmospheric ozone (O_3) decrease that could be caused by emissions of nitric oxide (NO) and nitrogen dioxide (NO_2) engine effluents from a large-scale operation of aircraft in the lower stratosphere. The assessment of the UV radiation increase at the earth's surface is an essential input for identifying engine characteristics to prevent a significant impact of stratospheric flight on the biosphere through UV-B radiation increases at wavelengths (λ) in the $280 \leq \lambda \leq 320$ nm range.[3]

The UV radiation increase at the earth's surface depends primarily on the magnitude of the emission index of NO_x (i.e., NO and NO_2 in g of NO_2/kg of fuel) in the engine effluents. In contrast with tropospheric flight experience, the physical factors that produce the UV radiation problem are:

1) Ozone has very strong absorption characteristics in the wavelength region below 320 nm. Therefore, it is one of the most important substances in the atmosphere for determining the level of UV radiation reaching the earth's surface; 2) A large fraction of the unperturbed atmospheric ozone column is stratospheric ozone, which is a trace gas with a concentration relative to stratospheric air of the order of 10^{-6}; 3) The residence times of NO_x effluents in the stratosphere are very long compared with those in the troposphere, a result that stems from the effect, on vertical transports, of the stratospheric temperature inversion from ozone heating; 4) The catalytic role of NO_x in the chemical destruction of ozone is significant. The NO_x in the unperturbed stratosphere is also a trace gas with a concentration relative to stratospheric air of the order of 10^{-9}

The stratosphere is the atmospheric layer extending from the tropopause to about 50 km altitude. The average tropopause height is a function of latitude, i.e., it varies from about 16 km at low latitudes to about 8 km at the poles. The formation of ozone is the result of mutual interactions among the solar radiation, photochemistry, chemical kinetics, and dynamics in the stratosphere. Therefore, the assessment of the potential UV radiation increase due to the effect of NO_x effluents on ozone requires an understanding of these complex interactions in the stratosphere. In fact, predictions of the potential UV radiation increase from NO_x engine effluents can only be based on the use of models of the stratospheric processes, because of the following two factors: 1) Proper simulation of the relevant couplings of stratospheric phenomena in the laboratory is not feasible, because of the large number of degrees of freedom in the complex stratospheric phenomena; and 2) The potential UV radiation increases would take place in a rather distant future after the initial operation of a worldwide fleet of aircraft in the lower stratosphere. The time scale for the UV radiation increase is controlled by a) the advent of a large-scale operation of supersonic aircraft in the lower stratosphere at altitudes between about 17 and 20 km (56-66 kft), and b) the time lag for an equilibrium response of the ozone decrease to an initial and continuous large-scale injection of NO_x effluents in the lower stratosphere. The equilibrium response would tend to duplicate the ozone decrease seasonally, assuming that the operation of aircraft in the lower stratosphere remains constant. The time to reach the equilibrium response of the zone decrease is calculated to be of the order of 5-7.5 yrs. Because of this long time lag, even an immediate escalation in the operation of aircraft in the lower stratosphere would not cause an early equilibrium (i.e., maximum) perturbation of the UV radiation at the earth's surface.

Only valid models of the couplings among radiative, chemical, and dynamical processes in the stratosphere can, therefore, provide correct and timely identification of potential adverse effects on the biosphere from the operation of aircraft in the lower stratosphere. The importance of this timing is emphasized further by the long time scales that are usually associated with the development and flight qualification of aircraft engine subsystems.

Basic requirements for the validation of these models are then as follows: 1) the models must at least simulate accurately the observed latitudinal and monthly variations of the UV radiation at the earth's surface as well as those of the atmospheric ozone column; 2) the models must minimize the use of empirical assumptions based on observed (i.e., unperturbed) conditions, especially for the consideration of

Henry Hidalgo is a member of the technical staff, Science and Technology Division, IDA. He was a research engineer in the preliminary design of airbreathing engines at the United Aircraft Research Department (1951-1954) and the Small Aircraft Engine Department of the General Electric Company (1954-1956). He was a principal research engineer at the AVCO/Everett Research Laboratory during the development of the intercontinental ballistic missile (ICBM), and published papers in hypersonic boundary layers and ablation (1956-1962). He was a consultant to aerospace companies (1962-1964) before joining IDA in 1964. He received an M.S. in mechanical engineering from the Massachusetts Institute of Technology (1951). He has been a member of the AIAA Technical Committees on Entry Vehicles as well as on Launch Vehicles and Missiles. He is an Associate Fellow of the AIAA.

Presented as Paper 75-335 at the AIAA 11th Annual Meeting and Technical Display, Washington, D.C., February 24-26, 1975; submitted March 5, 1975; revision received August 4, 1975. Although this paper is based on work done during the Climatic Impact Assessment Program of the Department of Transportation, this paper does not indicate endorsement by either that Department or by the Institute of Defense Analyses, nor should the contents be construed as reflecting the official position of either the Department or the Institute.

Index categories: Atmospheric, Space, and Oceanographic Sciences; Airbreathing Propulsion, Subsonic, and Supersonic; Thermochemistry and Chemical Kinetics.

large perturbations; and 3) the models must avoid the use of mathematical assumptions that would introduce spurious numerical effects. Subsequent sections describe the methodology for the assessment of the UV radiation increase and ozone decrease caused by the NO_x engine effluents.

UV Radiation at the Earth's Surface

Unperturbed UV Radiation

The characteristics of the observed UV radiation at a given wavelength are governed by the following independent factors: 1) solar zenith angle or obliquity of the illumination incident at the top of the atmosphere; 2) absorption by ozone, whose concentration reaches a maximum in the middle stratosphere; 3) absorption by aerosols in the stratosphere and troposphere; 4) scattering by the molecular and nonmolecular (i.e., aerosols and clouds) atmospheric constituents; and 5) reflection by the planetary surface.

The total flux (F_T, watts/m^2-nm or photons/sec-m^2-nm) of UV radiation reaching the earth's surface is the sum of the fluxes associated with the direct solar beam (F_S) and the diffuse sky radiation (F_D) i.e.

$$F_T = F_S + F_D \tag{1}$$

The attenuation of the UV radiation in a pure molecular atmosphere* is describable by a suitable vertical coordinate defined by

$$d\tau_\lambda = -[\sigma_{a,\lambda} n_a(z) + \sigma_{s,\lambda} n_s(z)]\, dz \tag{2}$$

where τ is a dimensionless optical thickness, subscript λ the wavelength of solar radiation, $\sigma_{a,\lambda}$ the absorption cross section, $n_a(z)$ the number density of the absorbing molecules (i.e., ozone) as a function of altitude (z), $\sigma_{s,\lambda}$ the single scattering cross-section, $n_s(z)$ the number density of scattering molecules (i.e., ozone and air), and z the height above the earth's surface. The values of $\tau(z)$ are obtained directly from integrating Eq. (2) for specified vertical distributions of $\sigma_{a,\lambda}$, $\sigma_{s,\lambda}$, $n_a(z)$, and $n_s(z)$. The range of τ between the top of the atmosphere and the ground is then $0 < \tau < \tau_g$. Table 1 shows typical values of the optical thickness at the ground a s a function of the magnitude of the total ozone amount (Ω) is an atmospheric column and the wavelength.

The direct flux of UV radiation at the earth's surface can be calculated from Bouger-Langley's (Beer's) law, i.e.

$$F_S = F_0 \cos\zeta_0 \exp(-\tau_g \sec\zeta_0) \tag{3}$$

where F_0 is the flux incident at the top of the atmosphere in a specified wavelength interval (1 nm), on a unit area held normal to the solar beam, and ζ_0 is the solar zenith angle. Thus, the direct flux can be readily calculated if the extraterrestrial value of the flux (F_0) and the extinction (absorption plus scattering) optical thickness (τ_g) for the specific wavelength and ozone amount are given along with the angle of solar illumination (ζ_0).

The diffuse flux of UV radiation, caused by multiple-scattering, can be calculated from the radiative transfer equation.[5-7] The calculation procedure involves the numerical solution of the integro-differential equation of radiative transfer in a modified spherical coordinate system, i.e., a triple integration over the zenith angle ($0 \le \zeta \le 90°$), the azimuth angle ($0 \le \varphi \le 360°$), and the optical depth ($0 < \tau < \tau_g$). Therefore, these calculations are more involved than those for the direct flux, and have to be repeated for each wavelength (λ), and each value of the independent variables for a pure molecular atmosphere, i.e., the solar zenith angle ($\mu_0 \equiv \cos\zeta_0$), total ozone amount (Ω), and ground reflectivity or albedo (A).

*A pure molecular atmosphere corresponds to a cloudless sky and minimum (local) aerosol content in the atmosphere. These conditions yield maximum absolute values of the UV radiation flux at the earth's surface.

Table 1 Optical thickness for UV radiation in a molecular atmosphere[4]

Ozone amount (m-atm-cm = 10^3 cm)[a]	Wavelength (nm = 10^{-9} m)	Optical thickness at ground (τ_g)
205	339.8	0.66
445	296.7	7.75

[a]If the atmospheric ozone column were compressed to a standard temperature and pressure (STP), the thickness of the ozone column would be, for example, 205 milli-centimeters or 0.205 cm.

Table 2 Ratio F_D/F_S in a pure molecular atmosphere. Ozone amount: 314 m-atm-cm. Reflectivity: 0.3[8]

λ(mn)	$\zeta_0 = 0°$	$\zeta_0 = 30°$	$\zeta_0 = 60°$
302.5	0.89	1.11	3.70
307.5	0.93	1.15	3.27
312.5	0.94	1.14	3.01
317.5	0.91	1.10	2.75
322.5	0.87	1.04	2.49

Table 2 illustrates the relative magnitudes of the calculated diffuse and direct fluxes for a pure molecular atmosphere as a function of the solar zenith angle and wavelength for a given value of the ozone column and reflectivity. This table shows that the diffuse flux is nearly equal to the direct flux at low solar zenith angles, and becomes significantly larger than the direct flux as the solar zenith angle increases. The effect of wavelength stems from the λ^{-4} variation of the Rayleigh scattering coefficient.

The numerical results for a pure molecular atmosphere indicate that for fixed values of the solar zenith angle and total ozone amount, the total flux of UV radiation increases as the wavelength increases in the range $280 < \lambda < 320$ nm. Thus, for a solar zenith angle of 36.9° ($\mu_0 = 0.8$) and ozone amount of 305 m-atm-cm, for example, the total flux of UV radiation increases by more than an order of magnitude as the wavelength increases from 300 to 320 nm. At any given wavelength, the total flux of UV radiation increases with a decrease in both the solar zenith angle and the total ozone amount. These results tend to be independent of the reflectivity in the range of interest ($0 < A < 0.3$).

The variation of the total UV radiation flux with latitude, month of the year, and local time of the day can be determined for a pure molecular atmosphere by: 1) calculating the direct and diffuse fluxes as a function of wavelength for a range of solar zenith angles, total ozone amount,and reflectivities; 2) using standard astronomical tables to obtain the solar zenith angle as a function of latitude, month of the year, and local time of the day; and 3) using measurements of the total ozone amount as a function of latitude and month of the year, (Fig. 1).

Results from such calculations give the daily variation of the total UV radiation flux during clear-sky days at any geographical location and month of the year. For example, such results indicate that the total flux at Albuquerque, New Mexico, during a clear July (summer) day reaches a maximum noontime value of about 3.3×10^{16} photons/m^2-sec-nm. Thus, the daily variation of the total flux can be used to determine a daily average value for a particular geographical location and month. The product of this daily average value and the number of seconds in a day (8.64×10^4 sec) yields the total amount of energy (number of photons), in a specified wavelength interval (1 nm), that is centered on a particular wavelength and is incident on a horizontal surface of unit area (1 m^2) during the sunlit hours. This procedure is used because the number of seconds in a day is constant throughout the seasons, whereas the sunlit hours vary with the seasons. Figure 2 shows isolines of the daily average of the total flux at $\lambda = 300.4$ nm, for example, for July (summer) over North America; the solid dots indicate the ozone observing stations.

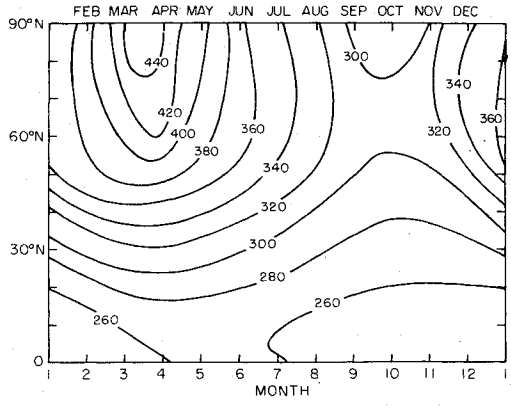

Fig. 1 Observed latitudinal and monthly variations of the zonal average of the ozone column (m-atm-cm) for the unperturbed stratosphere.[9]

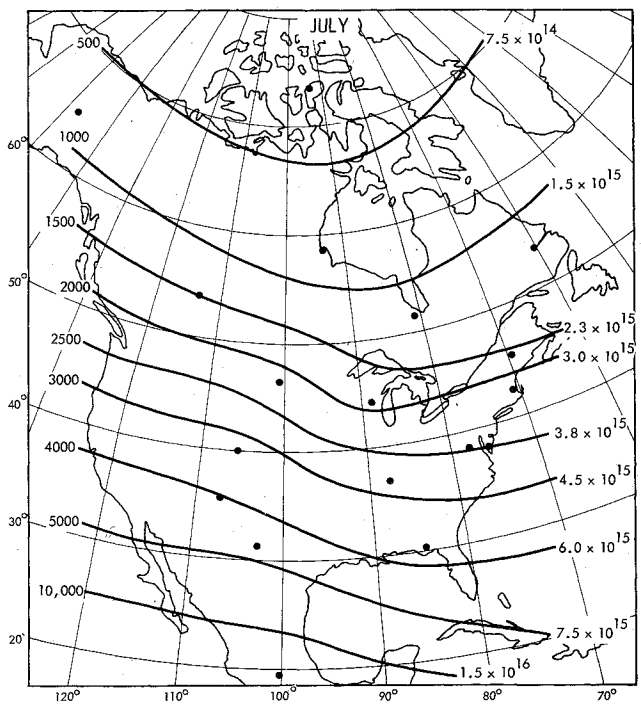

Fig. 2 Isolines of daily average flux at $\lambda = 300.4$ nm during summer (July). Units on the left are $\mu W/m^2$ nm and those on the right are in photons/m^2 sec nm.[8]

The results in Fig. 2 indicate that the daily average of the total flux increases by a factor of about 2 in the southern United States as compared with that in the north.

Figure 3 shows a typical comparison of the daily UV-B radiation during the year as obtained from a) observations for clear days at a given station by a Robertson meter, which measures the total UV-B radiation (i.e., integrated with wavelength in the region $280 < \lambda < 320$ nm) weighted by the erythemal action (i.e., response) spectrum through the use of a magnesium tungstate cell,[3] and b) corresponding calculations for a pure molecular atmosphere. The X's in the figure are obtained by multiplying the computed values by a factor of 1.1. This factor was determined from a least-square fit between observations and calculations. The remaining discrepancy between the X's and the circles is interpreted as being the result of the lack of simultaneous measurements of the UV radiation and ozone; i.e., from the use in the calculations of ozone amounts obtained from climatological data. Results such as those in Fig. 3 validate the methodology used in assessing the UV radiation increase caused by the ozone decrease from the NO_x effluents.

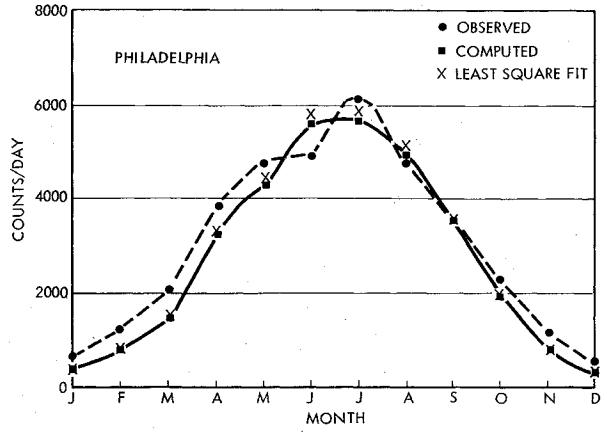

Fig. 3 Typical comparison between measurements of UV-B radiation (with Robertson meter) and corresponding calculations for a pure molecular atmosphere. Data is representative for several U.S. stations.[4]

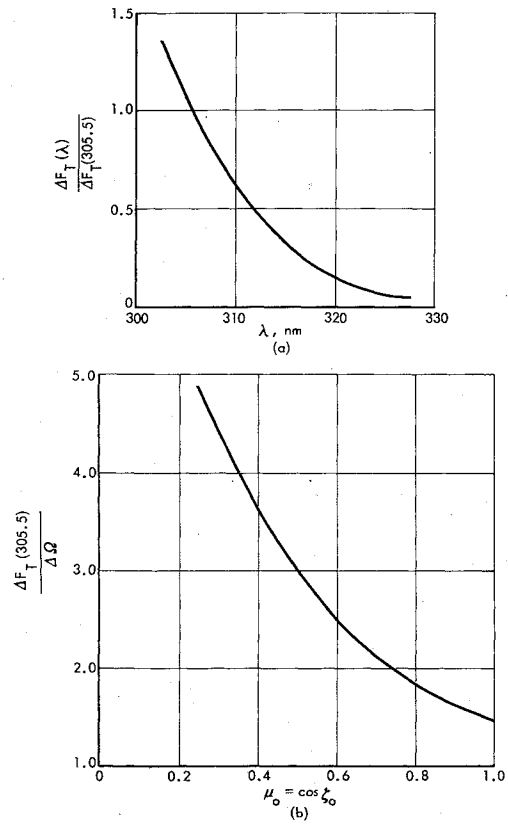

Fig. 4 Ratio of $\Delta F_T(\lambda)/\Delta F_T$ (305.5) versus wavelength and $-\Delta F_T(305.5)/\Delta\Omega$ vs cos ζ_0.[10]

Perturbed UV Radiation

The characteristics of the perturbed UV radiation are governed by the same physical factors as those for the unperturbed UV radiation. The UV radiation increase caused by the ozone decrease can then be expressed from Eq. (1) as

$$\Delta F_T \equiv \frac{\delta F_T}{F_T} = \frac{1}{1+F_D/F_S}\left[\frac{\delta F_S}{F_S} + \frac{F_D}{F_S}\frac{\delta F_D}{F_D}\right] \quad (4)$$

where ΔF_T denotes the fractional increase in the total flux of UV radiation in a given wavelength interval at the earth's surface, δ is a small change, F_D/F_S is the ratio shown in Table 2, and $\delta F_S/F_S$ and $\delta F_D/F_D$ are the respective fractional increases of the direct and diffuse fluxes.

The fractional increases of the direct and diffuse fluxes in a pure molecular atmosphere as a consequence of the fractional

Table 3 Percent increase in direct and diffuse fluxes for 2 percent decrease of the ozone column as a function of wavelength[8] ($\Omega = 305$ m atm cm, no ground reflection)

		Wavelength, λ, nm				
μ_0	Flux[a]	305.5	308.8	311.4	317.6	325.4
1.0	Δ^*F_S	2.65	1.91	1.27	0.54	0.16
	Δ^*F_D	2.92	2.16	1.48	0.68	0.22
0.8	Δ^*F_S	3.32	2.39	1.59	0.68	0.20
	Δ^*F_D	3.58	2.64	1.81	0.83	0.23
0.6	Δ^*F_S	4.45	3.20	2.12	0.91	0.27
	Δ^*F_D	4.65	3.42	2.33	1.06	0.33
0.4	Δ^*F_S	6.75	4.84	3.20	1.37	0.40
	Δ^*F_D	6.34	4.74	3.26	1.48	0.46

[a] Flux in percent, i.e., $\Delta^*F = 10^2 \Delta F$.

Table 4 Percent increase in direct and diffuse fluxes at $\lambda = 305.5$ nm as a function of the percent decrease in ozone[8] ($\Omega = 305$ m atm cm, no ground reflection)

		Decrease of ozone column							
μ_0	Flux[a]	1	2	3	4	5	10	15	20
1.0	Δ^*F_S	1.32	2.65	4.00	5.37	6.60	14.0	21.7	29.9
	Δ^*F_D	1.45	2.92	4.41	5.92	7.45	15.5	24.1	38.6
0.8	Δ^*F_S	1.65	3.32	5.02	6.75	8.51	17.8	27.8	38.6
	Δ^*F_D	1.78	3.58	5.42	7.30	9.20	19.2	30.2	42.2
0.6	Δ^*F_S	2.20	4.45	6.75	9.10	11.50	24.3	38.6	54.6
	Δ^*F_D	2.30	4.65	7.05	9.51	12.00	25.5	40.6	57.5
0.4	Δ^*F_S	3.32	6.75	10.30	14.00	17.80	38.6	63.2	92.2
	Δ^*F_D	3.12	6.34	9.70	13.10	16.60	36.0	58.6	84.0

[a] Flux in percent, i.e., $\Delta^*F = 10^2 \Delta F$.

Table 5 Balance between ozone production and destruction in the natural stratosphere[14]

Mechanism	Reactions (table in appendix)	Relative ozone rate (percent)
Photolysis of oxygen	1,2	100
NO_x catalytic cycle	6,7	−70
Ozone recombination	4	−17
HO_x catalytic cycles	58,59; 67,70,71	−12
Transport to earth's surface	...	−1

decrease in total ozone amount ($-\Delta\Omega$) have been determined numerically over a range of solar zenith angles for the following conditions: 1) a range of wavelengths at a fixed ozone decrease and ozone amount (i.e., Table 3); and 2) a range of the ozone decrease for a fixed wavelength and the same ozone amount (i.e., Table 4). The dependence of the fractional increase in total flux on wavelength, solar zenith angle, and ozone decrease may then be obtained from these results with fairly good approximation. Since F_D/F_S appears in the numerator and denominator of the expression for ΔF_T, Eq. (4) gives results that are insensitive to F_D/F_S. Using either the results in Table 2 or $F_D/F_S \simeq 1$, the results in Table 3 may be represented by the expression

$$\frac{\Delta F_T(\lambda)}{\Delta F_T(305.5)} = f(\lambda) \tag{5}$$

i.e., the ratio $\Delta F_T(\lambda)/\Delta F_T(305.5)$ displays a common wavelength dependence for all values of μ_0. Similiarly, the results in Table 4 yield the approximate expression

$$-\frac{\Delta F_T(305.5)}{\Delta\Omega} = g(\mu_0) \tag{6}$$

i.e., the ratio $-\Delta F_T(305.5)/\Delta\Omega$ shows only a weak dependence on the ozone decrease for each solar zenith angle. Figures 4a and 4b show, respectively, the function $f(\lambda)$ and $g(\mu_0)$. The combination of Eqs. (5) and (6) then yields

$$-\frac{\Delta F_T(\lambda)}{\Delta\Omega} = f(\lambda)\cdot g(\mu_0) \tag{7}$$

Equation (7) indicates that the percent increase in the total flux of UV radiation at the earth's surface, at a given wavelength and solar zenith angle for clear-sky conditions, is proportional to the percent ozone decrease in a range up to about 20% ozone decrease (Table 4).

One of the impacts of the increase in total UV radiation at the earth's surface caused by NO_x effluents in the stratosphere would be an increase in the erythemal dose for the sunburn-producing effect on Caucasian skin. If $E(\lambda)$ denotes an erythemal efficiency as defined by the Commission Internationale de l'Eclairage, the erythemal dose D can be represented by

$$D = \int E(\lambda) F_T(\lambda)\, d\lambda \tag{8}$$

The ratio of the fractional increase in the erythemal dose ΔD ($\equiv \delta D/D$) to the fractional ozone decrease can be written as

$$\frac{\Delta D}{\Delta\Omega} = \frac{\int E(\lambda)\cdot[\Delta F_T/\Delta\Omega]\cdot F_T(\lambda)\, d\lambda}{\int E(\lambda)\cdot F_T(\lambda)\cdot d\lambda} \tag{9}$$

Thus, for example, if the erythemal efficiency $E(\lambda)$ were concentrated solely at the peak of the erythemal response, $\lambda = 307.5$ nm, the approximate resulting increase in $\Delta D/\Delta\Omega$, at a latitude where the solar zenith angle at noon is 36.9° ($\mu_0 = 0.8$), would be $\Delta D/\Delta\Omega \simeq \Delta F_T(\lambda)/\Delta\Omega = (0.81)(-1.85) = -1.50$; consequently a 10% decrease in the ozone column would lead to a 15% increase in the erythemal dose D.

Ozone Column at the Earth's Surface

Unperturbed Ozone Column

The characteristics of the observed or unperturbed ozone column are shown in Fig. 1, which indicates that the zonal (i.e., longitudinal) average of the ozone column is a function of latitude and time of the year. The vertical concentration of ozone reaches a maximum value just above 20 km at middle latitudes.[9] Thus, a large fraction of the ozone column comprises stratospheric ozone.

The main physical characteristics in the global distribution of stratospheric ozone are the photochemistry initiated by solar radiation, the chemical transitions produced by chemically active species, and the large-scale quasi-horizontal dynamics of the stratosphere. Ozone is almost exclusively formed by the photolysis of oxygen, a process in which solar UV radiation is absorbed and a warming of the stratospheric air results. Thus, the vertical temperature gradient in the atmosphere changes from a negative value of about 6.5°C/km in the troposphere to positive values in the stratosphere. The temperature inversion in the relatively dry and cloudless stratosphere produces smaller rates of vertical mixing, com-

pared with those of the troposphere, and brings about a long residence time (of the order of a few years, depending on altitude) for trace substances injected into the lower stratosphere. The quasi-horizontal, large-scale dynamics of the stratosphere have a characteristic time scale of the order of a month, as established by the general circulation of air in the atmosphere. Therefore, a continuous, large-scale operation of aircraft in the lower stratosphere could result in the slow accumulation and global dispersion of NO_x effluents as a consequence of both the long residence time and the quasi-horizontal dynamics of the stratosphere.

The chemistry of the unperturbed ozone column is given mainly by the Chapman reactions for the O_x family [i.e., O_3, O_2, $O(^1D)$, $O(^3P)$] and the catalytic reactions involving the NO_y species [NO_x and nitric acid (HNO_3)], which occur in the middle and upper stratosphere. The NO_y species in the unperturbed stratosphere are a result of reactions involving mainly nitrous oxide (N_2O), which is diffused upward from the troposphere. The average global production of nitric oxide (NO) by this mechanism has been estimated at between 2.5×10^7 and 1.5×10^8 molecules /cm^2-sec,[11-13] The ionization of N_2 by cosmic rays can also lead to the production of nitric oxide. Between the 60° latitude and the pole, the mechanism is important from 10 to 30 km, and in the winter polar region it seems to be the only formation process of NO in the stratosphere. A possible third process is the oxidation of ammonia (NH_3) by OH radicals.

The equilibrium concentration of the unperturbed stratospheric ozone then depends on the balance between the production and destruction of ozone. The production of ozone is initiated by the photolysis of molecular oxygen (reaction 1, table in the appendix) and is continued by the chemical kinetics of O and O_2 (reaction 2). The destruction of ozone occurs mainly through the NO_x catalytic cycle (reactions 6 and 7), where the net effect is the destruction of ozone only. Other ozone destruction mechanisms are given by the recombination of ozone (reaction 4) and those produced by the HO_x (H, HO, HOO) free radicals based on water (reactions 58, 59, 67, 70, and 71). This balance is shown in a global basis in Table 5.

The role that the quasi-horizontal stratospheric motions plays in the global distribution of ozone is evident in Fig. 1. In the summer hemishere, the local rate of photolysis of molecular oxygen between 30 and 50 km varies in the range of $1 \times 10^6 < \partial[O_2]/\partial t < 5 \times 10^6$ molecules/cm^3 sec, a rate that increases with increasing altitude and tends to be independent of latitude. In the winter hemisphere, this local rate of photolysis above 30 km decreases within the above range with increasing latitude up to middle latitudes; at higher latitudes, $\partial[O_2]/\partial t \to 0$, a condition that prevails at every altitude in the high latitudes of the polar night. Yet, the results in Fig. 1 show that the values of the ozone column at high latitudes are larger during winter than during summer. Thus, ozone is transported poleward from the ozone formation region at low latitudes by the large-scale quasi-horizontal motions in the stratosphere.

A characteristic time for the stratospheric chemistry can be obtained from the ratio of the observed local concentration of ozone $[O_3]$ to the local rate formation of ozone, $\partial[O_3]/\partial t$, by photochemical processes, i.e., by using $\partial[O_3]/\partial t = 2\partial[O_2]/\partial t$. The magnitude of the chemical characteristic time is of the order of a week at 30 km altitude, shorter at higher altitudes, and considerably longer at lower altitudes. Thus, the chemistry has a predominant role in the middle and upper stratosphere, whereas the dynamics of the large-scale motion is of crucial importance in the middle and lower stratosphere (i.e., in the 15-25 km region).

General Circulation Model

The general circulation of air in the atmosphere is characterized by the variability of the air motion in both time and space, a variability that is larger in the stratosphere than in the troposphere. The observed statistics of the general circulation can then be represented by meridional and zonal circulations as well as eddy motions.[15] If $X(t, \theta, \Lambda, p)$ denotes a dependent variable that is a function of time (t), latitude (θ), longitude (Λ) , and pressure (p) or height (z), then the longitudinal or zonal average of X is denoted by $[X]$. Thus, $X = [X] + X^*$, where X^* is the deviation from the zonal average. The operation $[X]$ is associated with the zonal-mean circulation and X^* with the eddy motions. Similarly, the time average of X over, say, a month or season is denoted by $\bar{X}$. Hence, $X = \bar{X} + X'$, where $\bar{X}$ is associated with the standing motion and X' with the transient motion. The poleward motion, for example, with X equal to the northward wind (v) yields $v = [\bar{v}] + [v]' + \bar{v}^* + v^{*\prime}$ and the poleward transport of X (say, $X = O_3$) is then given by[16]

$$\overline{[Xv]} = [\bar{X}][\bar{v}] + \overline{[X]'[v]'} + [\bar{X}^*\bar{v}^*] + \overline{[X^{*\prime}v^{*\prime}]} \quad (10)$$

A main characteristic of the large-scale dynamics in the stratosphere is the dominant role of the horizontal eddy transports over the vertical motions.[17] Therefore, in contrast with the usual modeling of advective (mesoscale) phenomena in the troposphere, the characteristics of the large-scale motions in the stratosphere indicate an essential need to account for both the vertical and horizontal eddy motions in models of stratospheric dynamics.

The most general formulation for determining the ozone column must be based on the so-called primitive equations of the atmospheric motions†[16]

$$dU/dt = -fk \times U - g\nabla z + F \quad (11)$$

$$dT/dt = kT\omega/p + Q/c_p \quad (12)$$

$$\nabla \cdot U + \partial\omega/\partial p = 0 \quad (13)$$

$$\partial z/\partial p = -RT/gp \quad (14)$$

$$dR_i/dt = P_i - L_i \quad (15)$$

Equations (11-15) represent, successively, the conservation of momentum, energy, air mass, the approximate condition of hydrostatic equilibrium, and the conservation of the mixing ration (R_i) of trace species in the atmosphere. Equation (11) contains two scalar equations for the east-west and north-south motions. It represents the total or individual acceleration of the horizontal wind vector in terms of the coriolis acceleration due to the earth's rotation, the acceleration due to the geopotential (gz) gradients along surfaces of constant pressure, and the acceleration due to friction. The energy equation represents the total time rate of change of the air temperature (T) on the left-hand side, whereas the, as yet, undefined variables $\omega (\equiv dp/dt)$ and Q are related, respectively, to the vertical wind and the net heating rate per unit mass. The latter term provides a coupling among the radiative, thermal and dynamical processes in the stratosphere. The symbol R in Eq. (15) denotes the ratio n_i/n, where n_i is the number concentration (molecules/cm^3) of the i^{th} trace constituent and n is that of air. Therefore, Eq. (15) represents a subsystem of equations fixed by the number of the species (n_i). The terms P_i (production) and L_i (loss) on the right-hand side denote, respectively, the local production and destruction rates of species resulting, in general, from phase changes (e.g., water), precipitation, deposition, chemical reactions, etc. The expansion of the individual differential on the left-hand side of Eq. (15) shows then the coupling between the large-scale dynamics and the chemistry.

†Because of the emphasis on methodology, the intent here is for the average reader to primarily concern himself with the structure (and not the derivation) of all the basic equations.

The foregoing formulation of a general circulation model that couples the large-scale dynamics and the ozone chemistry is completed with the specification of the chemical species (n_i), and chemical reactions with associated data for the calculation of the production and loss terms in Eq. (15) for each chemical species. A complete list of 130 reactions, which need to be considered in modeling the stratosphere, is given in CIAP monograph 1.[18] The absorption cross sections, quantum yields, and reaction rates for this set of reactions are given by the National Bureau of Standards compilation in CIAP monograph 1. The list of 130 reactions can be reduced to 55 important ones, which are identified by the underlined numbers of the reactions in the table shown in the appendix. It is feasible to further reduce the number of the important reactions from 55 to 34 reactions and 17 species.[19] The 17 species include the O_x family [O_3, O_2, $O(^1D)$, $O^3(P)$], the NO_z family‡ [N_2, N, N_2O, NO, NO_2, NO_3, HNO_3, HNO_2], and the HO_x family [H_2O, H, HO, HOO, and H_2O_2].

The system of Eqs. (11-15) must be solved numerically using appropriate initial and boundary conditions. The numerical integrations of these equations require the use of several vertical or pressure levels between the earth's surface and the upper stratosphere, a condition that usually defines the vertical resolution of the model at 3 km. In the horizontal domain, these integrations require a definition of horizontal numerical grids over each global surface of constant pressure. The capabilities of current computers allow the use of a horizontal grid resolution of the order of 250 km to solve the system of Eqs. (11-14), i.e., for the stratospheric circulation without chemical interactions. The zonal and time averages of these numerical solutions then provide computed results for the meridional circulation and eddy motions [Eq. (10)].

The Geophysical Fluid Dynamics Laboratory (GFDL), Princeton, N.J., general circulation model (GCM) has provided approximate numerical solutions of the system of Eqs. (11-15) for an arbitrary, chemically inert tracer with a simulated continuous source located at the 65-mb pressure level at the northern midlatitudes during the winter (January).[17,20] The vertical domain of the model extends from the ground to about 30 km, and it has a vertical resolution of 3 km. These results are based on the solution of Eq. (15) for the inert tracer, an equation that utilizes as inputs available solutions for the dynamics from the system of Eqs. (11-14). These numerical solutions show the meridional distribution of the inert tracer after integrations for 18 months, a distribution that has reached the equilibrium values except in the southern hemisphere and at high northern latitudes.[1,21] The equilibrium distribution of the inert tracer is useful for evaluating the equilibrium distribution of the NO_y species, which has been derived from approximate models, (described in the next section), of the stratospheric dynamics.

Stratospheric Circulation Model

The limitations of available computers have prevented the solution of the system of Eqs. (11-15), even with the foregoing simplified chemistry for the O_x, NO_z, and HO_x species. Therefore, it has been necessary to introduce approximations in this system, as described below, for the development in the short time scale (~3 yrs) of CIAP of a stratospheric circulation model (SCM) at the Massachusetts Institute of Technology (MIT).[22]

A first approximation is the use of the condition of geostropic equilibrium, which is a feature of the general circulation of air at middle and higher latitudes that is almost as prominent as the hydrostatic equilibrium. The geostrophic equilibrium is produced by the approximate balance between the coriolis and geopotential terms on the right-hand side of Eq. (11). Just as the condition of hydrostatic equilbrium filters out the vertically traveling sound waves (which are unimportant for the general circulation), the condition of geostrophic equilibrium filters out the oscillations due to gravity waves, which are of questionable importance for the global circulation.[16]

A second approximation is to use a horizontal resolution that is coarser than that of the available GCMs based on the primitive equations. The MIT SCM, based on the geostrophic approximation, represents the dependent variables (e.g., winds, temperature, etc.) in the spectral domain using spherical harmonics. The horizontal resolution of the SCM depends then on the number of the spherical harmonics used in the representation of the dependent variables. The MIT SCM uses 79 spherical harmonics, which yields a horizontal resolution of the order of 1,500 km at midlatitudes, i.e., a factor of about six coarser than that of the GFDL GCM. The vertical levels extend from the earth's surface to 70 km altitude, i.e., to include the upper mesosphere while maintaining the same vertical resolution (3 km) as the GFDL GCM. The tradeoff between the horizontal resolution and computing time is rather dramatic. The MIT SCM requires only 40 sec on an IBM 360/95 computer for a one-day simulation of stratospheric phenomena. A high-resolution GCM using the same computer would require longer times by at least two orders of magnitude. Thus, the MIT SCM has been able to simulte three annual cycles of the unperturbed and perturbed stratospheres, the latter as a result of a continuous injection of NO_x effluents at either 17 or 20 km altitude.

A third, and rather drastic, approximation in the MIT SCM is the use of one continuity equation, Eq. (15), for only ozone. This means that it is now required to use the equilibrium distribution of the NO_x effluents as an input for the SCM. Since this equilibrium distribution is obtained from a zonal average of the system of continuity Eqs. (15), the MIT SCM cannot further provide meaningful longitudinal effects for the ozone decrease. The set of chemical reactions directly included in the MIT SCM is, therefore, very limited; i.e., it consists of the Chapman reactions, the catalytic cycle of NO_x, and the HO_x reactions (as defined by reactions 1-4, 6, 7, 9, 59, and 71 in the table in the appendix). Since the input equilibrium distribution of NO_x is determined from a more extensive consideration of the chemistry (as indicated below), the MIT SCM accounts for the important effect of the NO_y species.

Two-Dimensional Stratospheric Models

The two-dimensional models utilize, in general, the zonal and time averages of the primitive equations themselves. The transient two-dimensional stratospheric models have utilized so far the zonal average of only the system of continuity Eqs.(15) for the chemical species. The result is then as follows:[23]

$$\frac{\partial[R_i]}{\partial t} + \frac{[v]}{a}\frac{\partial[R_i]}{\partial\theta} + [\omega]\frac{\partial[R_i]}{\partial p} + \frac{1}{a\cos\theta}\frac{\partial}{\partial\theta}\cos\theta\,[R_i^*v^*] + \frac{\partial}{\partial p}[R_i^*\omega^*] = [P_i - L_i] \tag{16}$$

The second and third terms on the left-hand side of Eq. (16) represent the transport of the mixing ratio by the meridional circulation. The fourth term represents the poleward eddy transport, and the fifth one the vertical eddy transport. This uncoupling of the subsystem of Eq. (15) from Eqs. (11-14) does not allow for interactions of the chemical perturbations with the temperature and dynamic perturbations of the stratosphere. Another basic assumption in the two-dimensional models is that the sum of the standing and transient eddy terms, i.e., third and fourth terms on the right-hand side of Eq. (10), is given by a diffusion vector and the

‡The following conventions have evolved in CIAP: NO_x to denote NO and NO_2, NO_y to specify NO_x and HNO_3. The NO_z is used here to denote the species in the above parenthesis.

appropriate gradient of the meridional circulation, e.g.

$$\overline{[X^*v^*]} = -\left[K_{yy}\frac{\partial[\bar{X}]}{\partial y} + K_{yz}\frac{\partial[\bar{X}]}{\partial z}\right] \qquad (17)$$

where y denotes northward distance. A similar expression is assumed for the vertical transports. The K_{yy}, K_{yz}, and K_{zz} coefficients are specified empirically as a function of month (or season), latitude and pressure level (or altitude).

The equilibrium distribution of NO_x effluents in the unperturbed and perturbed stratospheres to be used as input for the MIT SCM is obtained by Prinn et al. from numerical solutions of Eq. (16) for N_2O, NO_y, and HNO_3.[§24] The statistics of the general circulation are prescribed, based on the data of Gudiksen et al. for the meridional circulation and the K_{yy}, K_{yz}, and K_{zz} coefficients.[25] The Gudiksen et al. data are based on the observed movement of tungsten-185 radioactive debris that had been injected into the tropical stratosphere in 1958. The chemistry used in these calculations is identified in the table shown in the appendix. These calculations do not predict ozone, but use instead observed ozone concentrations. The use of the observed ozone for the prediction of N_2O, odd nitrogen, and odd hydrogen in the perturbed atmosphere is based on the expected inability of the two-dimensional model to predict ozone concentrations with an accuracy better than the magnitude of the ozone decrease from the SCM. The vertical domain of this two-dimensional model is $8<z<38$ km with a vertical resolution of 1 km. The time integrations are performed until the long-lived species reach an equilibrium value. Thus, the equilibrium distributions of the NO_x effluents take into account the effect of seasons on both the annual cycle of the solar radiation and the large-scale dynamics.

The relative effect of the Prinn two-dimensional model parameterization¶ of the large-scale motion on ozone reduction can be assessed from solutions of Eq. (16) with different values of the meridional circulation and K coefficients. Another transient two-dimensional model developed by Widhopf solves the continuity equations for 14 species, i.e., the O_x, NO_z, and HO_x species identified earlier.[26] Two additional species, H_2O and CH_4, are also considered, but they are fixed in time through the use of experimental data. The chemistry used in this model is identified in the table shown in the appendix. In contrast with the Prinn two-dimensional model, the Widhopf two-dimensional model does solve for the ozone decrease. The Widhopf two-dimensional model uses the meridional circulation derived by Louis[27] from the zonal averages of Eq. (12) and (13) together with appropriate observed temperature fields. The eddy transports used in this model have been obtained by Luther[27] from measurements (up to $z<20$ km) and extrapolations ($z>20$ km) of heat flux, temperature, and wind variance data compiled for 1958-1963 by Oort and Rasmusson.[15] Therefore, the parameterized motion used in the Widhopf model does not depend on the type of trace substances injected into the stratosphere. The vertical domain of this model is $10<z<50$ km, with a vertical resolution as in the Prinn model. The time integrations are performed with a constant dynamics that is representative of the autumn season (October) in the northern hemisphere and the spring season (April) in the southern hemisphere.

One-Dimensional Stratospheric Models

Because of the predominant role of the horizontal eddy motion in the stratosphere,[17] the one-dimensional model for the stratospheric dynamics must be based on global averages of the continuity Eq. (15). Using the altitude instead of the pressure coordinate, the result then is:

$$\frac{\partial\tilde{\rho}\tilde{R}_i}{\partial t} = \frac{\partial}{\partial z}\tilde{\rho}K_z\frac{\partial\tilde{R}_i}{\partial z} + \tilde{\rho}\tilde{P}_i - \tilde{\rho}\tilde{L}_i \qquad (18)$$

where the symbol $\sim$ denotes the global average operation, ρ the air density, and K_z the one-dimensional parameterization of the stratospheric motion given by

$$\tilde{wR}_i = -K_z\frac{\partial\tilde{R}_i}{\partial z} \qquad (19)$$

in which w denotes the vertical wind. Equation (19) indicates that the one-dimensional parameterization of the stratospheric dynamics, $K_z(z)$, must be obtained from the ratio of the global average of the vertical flux of the mixing ratio to the vertical gradient of the global average of the mixing ratio. Several one-dimensional models have been developed to investigate the effect of chemistry and the K_z profile on ozone.[23] The Chang model, for example, uses a K_z profile based on average K_z values from the data by Gudiksen et al.[25] on the observed movement of tungsten-185 radioactive debris. The chemistry used in the Chang model is also identified in the table shown in the appendix.

Results for the Unperturbed Ozone Column

The degree of validity of the MIT SCM/two-dimensional model for the unperturbed stratosphere can be assessed from the results in Fig. 5 for the unperturbed ozone column.[22,28] These results were obtained after time integrations of three years in the SCM, which started with an atmosphere at rest and utilized the equilibrium distribution of NO_x. Time increments of one hour are used in the SCM, and an integration time of two years is required for the stratospheric values to attain their equilibrium values. Figure 5 shows that this model simulates, with reasonable accuracy, both the magnitude of the observed ozone column as well as its variations with latitude and time of the year (see Fig. 1). The accuracy of this numerical simulation is somewhat dependent on the parameterization of the vertical transport (K_{zz}) in the subgrid scale of the SCM. Since the Widhopf two-dimensional model also yield reasonable results for the unperturbed ozone and NO_y species during the fall and spring seasons, it has not yet been possible to assess the relative accuracy of these two models. This is so because a conclusive evaluation of the ozone models must include accurate comparisons between the numerical simulation of the meridional distribution of the NO_y species as a function of seasons and the corresponding, but as yet incomplete, observed statistics [i.e., Eq. (10) with $X=NO_x$, etc.] for such species.[29]

Perturbed Ozone Column

The ozone chemistry for the perturbed stratosphere would be modified mainly by the addition of the NO_x engine effluents in the flight corridors of the lower stratosphere. Important mechanisms for the ozone column decrease, $\Delta\Omega$ in Eqs. (7) and (9), are the upward transport of the NO_x effluents to the middle stratosphere (20-35 km region, where chemistry is important) and the large-scale transports in the middle and lower stratosphere. Since the ozone decrease depends on the equilibrium distribution of the NO_x effluents in the middle stratosphere, the independent variables for the decrease of the ozone column, as a function of latitude and season (e.g., Fig. 1), are the strength and location of the aircraft NO_x sources; i.e., the annual, global injection rate of NO_x($\dot{E}_{NO_x}$, 10^9 kg/yr), and the altitude (z_c, km) as well as latitude (θ_c) of the flight corridors in the lower stratosphere.**

§The NO_x distributions for the unperturbed stratosphere were derived from earlier calculations by Hesstvedt, an expedient procedure that was necessary to meet CIAP deadlines while the development of the Prinn model was incomplete.[31]

¶The term "Parameterization" is used in meteorology as a contraction of "parametric representation" to denote an empirical, rather than physico-mathematical, description of atmospheric phenomena.

**The longitude of the flight corridor (e.g., New York-Buenos Aires) would only modify the latitudinal direction of the aircraft NO_x sources.

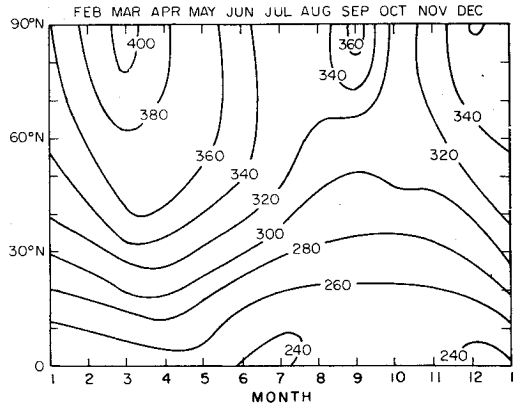

Fig. 5 Calculated latitudinal and monthly variations of the zonal average of the ozone column (m-atm-cm) for the unperturbed stratosphere.[22]

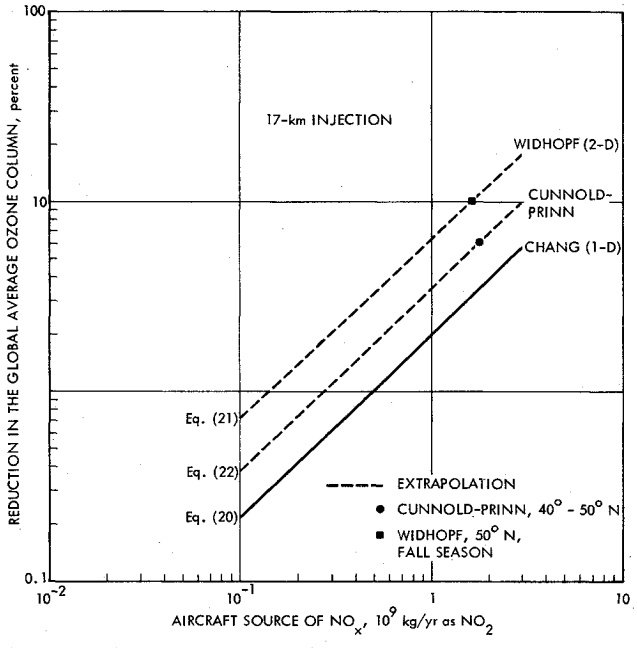

Fig. 6 Percent decrease of the global average of the ozone column as a function of the annual, global injection rate of NO_x effluents at 17 km altitude [omit 10^{-2} factor in Eq. (20) for the above results].[1]

The MIT SCM/two-dimensional results for the perturbed stratosphere indicate that the destruction of ozone by the NO_x catalytic cycle is slow at the altitude of the flight corridors in the lower stratosphere. The significant ozone destruction occurs after the NO_x has been transported upward to heights in excess of 25 km. Consequently, most of the ozone reduction occurs above 25 km, but this ozone reduction also has the effect of reducing the amount of ozone available to be transported to lower altitudes. The net effect is a reduction in ozone at all altitudes below 50 km. The only sink for the additional odd nitrogen is in the troposphere. The distribution of odd nitrogen in the stratosphere is controlled by the dynamics with most of the NO_x removal occurring in the region of the tropopause gaps.[22,30]

Figures 6 and 7 show the decrease in the global average of the ozone column for three model types as a function of the annual, global injection rate of NO_x effluents ($\dot{E}_{NO_x}$ in 10^9 kg/yr as NO_2) for flight corridors at 17 and 20 km altitudes. The former altitude is applicable to the Concorde and the latter to an advanced supersonic transport (SST).

The procedure used to obtain the one-dimensional results in Figs. 6 and 7 first requires determination of the unperturbed equilibrium solution for a fixed solar zenith angle of usually

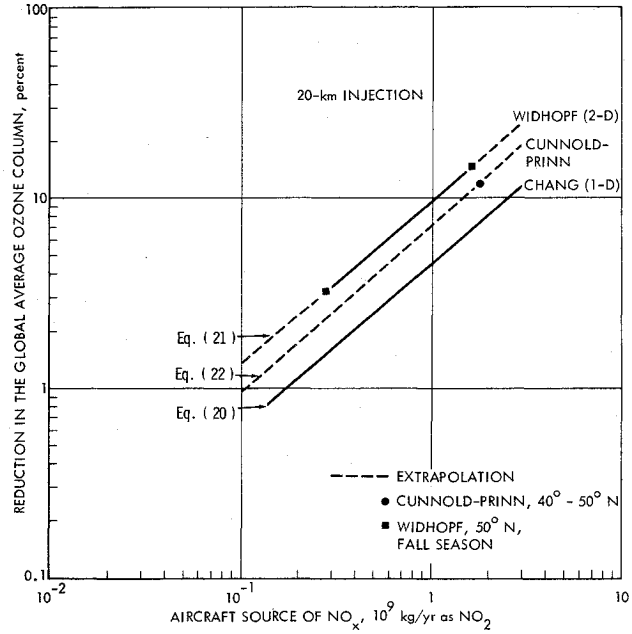

Fig. 7 Percent decrease of the global average of the ozone column as a function of the annual, global injection rate of NO_x effluents at 20 km altitude [omit 10^{-2} factor in Eq. (20) for above results].[1]

45°.[23] The equilibrium solution is essentially reached in this model after time integrations for 5 years. A given amount of NO_x effluence ($\dot{E}_{NO_x}$) is then introduced at a given altitude, and the effluents are distributed uniformly in a 1 km-thick spherical shell. After the integration with respect to time yields the perturbed equilibrium solution, the fractional decrease in the ozone column can be obtained from the unperturbed and perturbed solutions. The calculations are repeated for other NO_x injections to generate the fractional ozone decrease as a function of the annual, global injection rate of NO_x at a given altitude. The fractional ozone reduction from the Chang model may be represented by[1]

$$-\Delta\tilde{\Omega} = 10^{-2}[2+0.8(z_c-17)] \cdot \cdot [\dot{E}_{NO_x} \times 10^{-9}]^{[0.88+(0.07/3)(20-z_c)]} \qquad (20)$$

where $-\Delta\tilde{\Omega}$ is the fractional decrease in the global average of the ozone column, z_c the altitude of the flight corridor in the range $17 < z_c < 20$ km, and $\dot{E}_{NO_x}$ the annual, global injection rate of NO_x effluents in the range $0.1 < \dot{E}_{NO_x} \times 10^{-9} < 3$ kg/yr.

The Widhopf two-dimensional results in Fig. 6 and 7 take into account the effect of latitude on solar zenith angle.[23,26] The NO_x effluents are introduced in a zonal band, 1 km-thick and 10° wide, centered at the corridor altitude and at 50° N latitude to simulate a North Atlantic flight corridor. The calculations have been made for an NO_x injection rate of 1.65×10^9 kg/yr (as NO_2) at either 17 or 20 km altitude, and for one-sixth this value at 20 km to deduce the effect of the injection rate on the ozone decrease. This two-dimensional model has yielded the equilibrium values for the zonal average of the stratospheric ozone column ($10 < z < 50$ km) for the unperturbed and perturbed stratosphere with constant dynamics. The equilibrium values are obtained after time integrations for 7.5 years. Figures 6 and 7 show the decrease in the global average of the ozone column as determined from the difference of the integrations with respect to latitude of the unperturbed and perturbed zonal values. Figure 8a shows the decrease in the zonal average of the stratospheric ozone column in the Northern and Southern Hemispheres as a result of NO_x injections at 50°N latitude. Figure 8b displays the zonal results as normalized with the decrease in the corresponding global averages. This figure shows that the

normalized zonal ozone decrease tends to be independent of the strength or altitude location of the aircraft NO_x source at 50° N latitude. These two-dimensional results may be represented by[1]

$$\Delta\Omega_{2D} = [2.2 + 0.07(1.65 - \dot{E}_{NO_x} \times 10^{-9})] \cdot \cdot [1 + 0.14(20 - z_c)] F_\theta \Delta\tilde{\Omega} \quad (21)$$

where $\Delta\Omega_{2D}$ is the fractional decrease in the zonal average of the ozone column, F_θ the normalized factor given in Fig. 8b, and $\Delta\tilde{\Omega}$ is given by Eq. (20). A value of F_θ equals unity provides the ratio of the two-dimensional to one-dimensional decrease in the global average of the ozone column.

The Cunnold-Prinn et al. results in Figs. 6 and 7 are obtained from the MIT SCM and the auxiliary Prinn two-dimensional model for determining the equilibrium NO_x distributions.[22,30,31] These results are obtained after time integrations for three years in the SCM, which utilizes the equilibrium distribution of the perturbed NO_x derived from the Prinn two-dimensional model after time integrations for 25 years. These results thus take into account the effects of the latitudinal and seasonal variations of the solar radiation on the chemistry and large-scale dynamics. The available results consider an injection rate of NO_x of 1.8×10^9 kg/yr (as NO_2) between 40° and 50° N latitude at either 17 or 20 km altitude. Figure 9 shows the decrease in the zonal average of the ozone column in the northern and southern hemispheres for the 20 km altitude as a function of the seasons.[31] The MIT SCM/two-dimensional results may be represented by[1]

$$\Delta\Omega_{SCM/2\text{-}D} \simeq \left[1.6 + \frac{0.10}{3}(20 - z_c)\right] F_{\theta S} \Delta\tilde{\Omega} \quad (22)$$

where $\Delta\Omega_{SCM/2\text{-}D}$ is the fractional decrease in the zonal average of the ozone column, $F_{\theta S}$ is the normalized latitudinal (θ) and seasonal (S) factor shown in the right-hand side ordinate of Fig. 9, and $\Delta\tilde{\Omega}$ is given by Eq. (20). Again, a value of $F_{\theta S}$ equals unity provides the ratio of the SCM/two-dimensional to one-dimensional decrease in the global average of the ozone column. The factor $F_{\theta S}$ is a function of the altitude of injection, i.e., it tends to be a weaker function of latitude for injections at 17 km altitude compared with that in Fig. 9 for the 20 km injection.

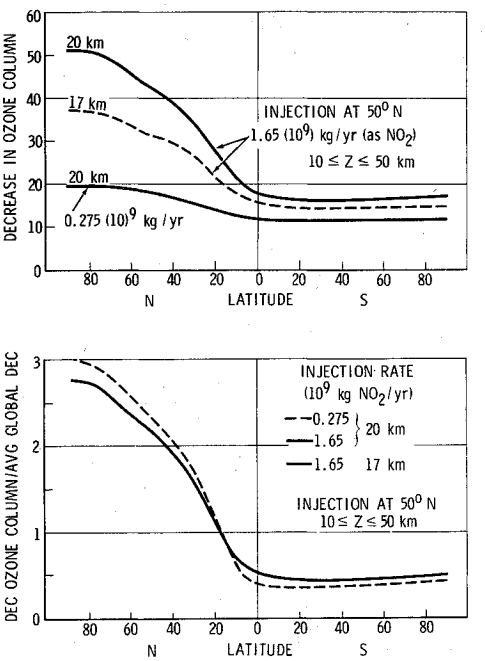

Fig. 8a) percent decrease of the zonal average of the ozone column for fall season as a function of NO_x injection conditions; b) same as a) but normalized with the global average of the ozone decrease.[26]

The annual, global injection rate of NO_x effluents in the expression for $\Delta\tilde{\Omega}$ in Eqs. (20) to (22) is given by the product of the annual fuel-flow rate during stratospheric flight and the emission index of NO_x; i.e., by the expression

$$\dot{E}_{NO_x} = 8.76 \times N \times E_p \times f \times \dot{W}_{fe} \times EI_{NO_x} \quad (23)$$

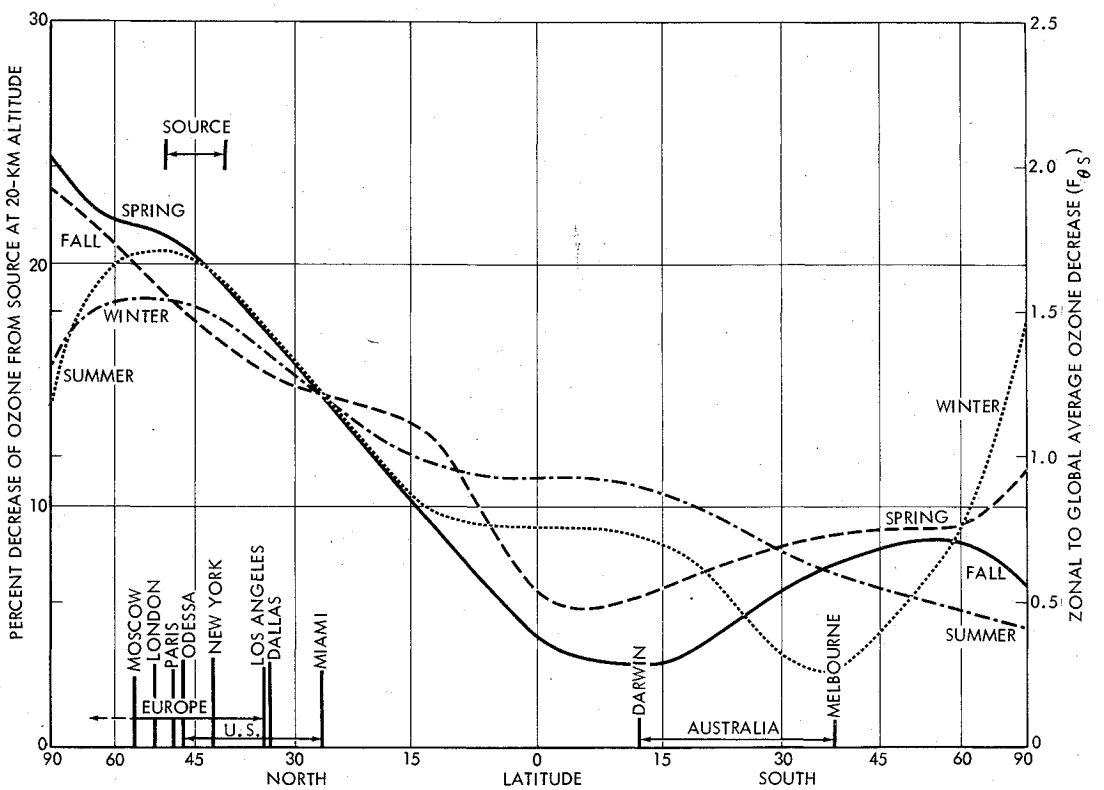

Fig. 9 Percent decrease of the zonal average of the ozone column as a function of seasons. $\dot{E}_{NO_x} = 1.8 \times 10^9$ kg/yr at 20 km altitude.[31]

Table 6 Fuel-flow projections for 1990 and 2000 in 10^9 kg/yr[32]

Altitude (km)	Expected traffic 1990	2000	Upper-bound traffic 1990	2000
9-12	43.7	75.0	81.6	193.9
12-15	15.3	29.8	28.5	76.1
15-18	0.7	1.8	1.4	5.6
18-21	14.6	37.4	26.2	110.6

Table 7 Ozone reduction from the SCM/2-D results as a function of the annual, global injection of NO_x

Flight corridor altitude	NO_x emissions	Ozone reduction (%) 45°N,	45°S,
(km)	(kg/yr)	summer	summer
20	1.8×10^9	20.5	6.7
20	1.8×10^8	2.7	0.9

where $\dot{E}_{NO_x}$ is given in kg/yr, N denotes the number of airplanes flying in a given corridor, E_p the number of engines per airplane, f the average fraction of the day that the airplanes fly at the corridor altitude, $\dot{W}_{fe}$ the average fuel-flow rate per engine (kg/hr-engine) during flight at the corridor altitude, and EI_{NO_x} the emission index of NO_x (g of NO_2/kg of fuel). The constant is the number of hours in a year divided by 10^3. An upper limit of $\dot{E}_{NO_x}$ can be obtained from optimistic (i.e., upper-bound) projections of the aircraft traffic in the stratosphere.

Table 6 summarizes projections of subsonic (9-15 km) and supersonic (15-21 km) airline traffic by the end of this century as given by CIAP monograph 2.[32] Since the annual, global injection rate of NO_x is given by the product of the fuel-flow rates in Table 6 and the NO_x emission index, it can be seen that the SCM/two-dimensional results and the two-dimensional results for the higher injection rate (Figs. 6 and 7) are near the maximum $\dot{E}_{NO_x}$ value, i.e., they correspond to the upper-bound supersonic traffic in the year 2000 with a 1974 NO_x emission index ($EI_{NO_x} = 18$ g of NO_2/kg of fuel).

The SCM/two-dimensional results in Fig. 6 indicate that the average magnitude of the decrease in the global average of the ozone column for a flight corridor at 17 km altitude varies linearly from about 0.7% for an NO_x (as NO_2) injection rate of 2×10^8 kg/yr to about 7% for an NO_x injection rate of 2×10^9 kg/yr. These reductions of ozone are average values, because they can be larger or smaller by a factor of about 2 as indicated by the two other model types in the same figure. This variation is mainly caused by the current uncertainty in the description of the stratospheric dynamics.

When the altitude of the flight corridor is increased from 17 to 20 km, the above average values for the reduction in the global average of the ozone column increase to about 1.7 and 13% for NO_x injection rates of 2×10^8 and 2×10^9 kg/yr, respectively, (Fig. 7). Again, these average values can be larger or smaller by factors of about 1.3 or 1.6, respectively, from the uncertainty in the description of the stratospheric dynamics.

The SCM/two-dimensional results in Fig. 9 together with Eq. (22) indicate that the decrease in the zonal average of the ozone column at middle northern latitude increases over that of the global average by a factor ($F_{\theta s}$) of about 1.7 during summer. Table 7 illustrates the relative effect of the strength of the aircraft NO_x source at the worse altitude (20 km) on the ozone decrease at middle latitudes during summer in both hemispheres. The results for the lower injection rate in Table 7 assumes that $F_{\theta S}$ is independent of the injection rate at the given altitude of injection, an assumption based on the Widhopf two-dimensional model results (Fig. 8b). The results in Table 7 and Eq. (23) indicate that a significant reduction in the NO_xemission index of aircraft engines would also result in a significant reduction of the ozone column decrease.

A comparison of the results in Figs. 8a and 9 indicates a significant discrepancy in the ozone decrease during the fall season at middle northern latitudes for nearly identical NO_x emissions at 20 km altitude. The resuts from the GFDL GCM for the meridional distribution of an arbitrary inert tracer can be used to assess the accuracy of the NO_y distributions from the SCM/two-dimensional and Widhopf two-dimensional models. A comparison of the GFDL GCM and the Prinn results indicate no significant difference between them, i.e., on the way to equilibrium, the Prinn model does, at one point, approximate the GFDL GCM 18-months result.[33] The best time for similar comparisons between the GFDL GCM and the Widhopf results is after the completion of ongoing calculations, using the Widhopf model, to account for the annual cycles of both solar radiation and dynamics as well as the effect of dropping the lower boundary to the earth's surface.††

Summary of Perturbed Ozone and UV Radiation Results

The combination of Eqs. (7) and (22) yields the total UV radiation increase as a function of the annual, global injection rate of NO_x effluents at middle northern latitudes, the corridor altitude, the latitude in both hemispheres, and the seasons. Since the injection rate of NO_x is proportional to the NO_x emission index (EI_{NO_x}) of aircraft engines [i.e., Eq. (23)], the UV radiation increase can be related to the level of this emission index. The methodology thus shows that 1) the UV radiation increase is approximately proportional to the ozone decrease in a range up to about 20% ozone decrease [i.e., Eq. (7)], and 2) the magnitude of the ozone decrease is nearly linear with the magnitude of the NO_x emission index of aircraft engines (Eqs. 22, 20, 23). Thus, a significant reduction of the NO_x emission index would lead to a significant reduction of the UV radiation increase (i.e., Table 7 and Eq.7).

Using Eq. (8) for the unperturbed and perturbed stratosphere and the results from the MIT SCM/two-dimensional model for the upper limit NO_x injection rate of 1.8×10^9 kg/yr at 20 km altitude between 40° and 50° N latitude, the corresponding erythemal dose increases during summer at 30° and 60° N are, respectively, 30 and 58%.[30,34] These changes in the erythemal doses would be similar to those now being received some 15° of latitude to the south. However, it must be emphasized that this result is based on the use of the projected upper-bound SST traffic for the year 2000 at 20 km altitude (e.g., Table 6) with aircraft engines that have an NO_x emission index based on 1974 engine technology (i.e., $EI_{NO_x} \simeq 18$ g of NO_2/kg of fuel).

A conclusive validation of the methodology for the UV radiation increase from the ozone decrease due to an increase in NO_x must yet overcome 1) the somewhat limited scope of observations concerning the statistics of the NO_y species (NO_x and HNO_3) in the unperturbed stratosphere,[29] and the unknown long term variations of the UV radiation at the top of the atmosphere. For example, computations from a one-dimensional model for the unperturbed stratosphere indicate an ozone increase of as much as 6% when the UV radiation is increased by 50% in the 175-200 nm range together with a 20% increase in the 200-240 nm range;[35] and 2) the present theoretical limitations of stratospheric circulation models concerning the vertical resolution in the model, the description of the ozone chemistry in the model, and the role of the large-scale dynamics in the equilibrium distribution of aircraft NO_x effluents in the middle stratosphere. The former limitations prevent the accurate matching of theoretical and observed NO_y profiles for the unperturbed stratosphere as a

††Recent results indicate that the SCM/two-dimensional results also agree with those obtained from a two-dimensional model developed by Crutzen.[36]

function of latitude and season; the latter one prevents taking into account feedback effects in the perturbed stratosphere, e.g., the cooling of the stratosphere from a significant ozone decrease on the ozone chemistry.[1,23]

Appendix

Reactions Used In Ozone Models[18,23,24,26]

	Chang[23]	Prinn[24]	Widhopf[26]
A. The Chapman or "pure air" reactions[a]			
* 1. $O_2 + h\nu$ (below 242 nm) → O + O	x	x	x
* 2. $O + O_2 + M \rightarrow O_3 + M$	x	x	x
* 3. $O_3 + h\nu \rightarrow O_2 + O$	x	x	x
* 4. $O_3 + O \rightarrow O_2 + O_2$	x	x	x
* 5. $O + O + M \rightarrow O_2 + M$			
B. Reactions of the oxides of nitrogen that enter the catalytic cycles for ozone formation destruction			
* 6. $NO + O_3 \rightarrow NO_2 + O_2$	x	x	x
* 7. $NO_2 + O \rightarrow NO + O_2$	x	x	x
* 8. $NO_2 + O + M \rightarrow NO_3 + M$			
* 9. $NO_2 + h\nu$ (below 400 nm) → NO + O	x	x	x
10. $NO_2 + h\nu$ (below 245 nm) → NO + O(^{1}D)			
*11. $NO + NO + O_2 \rightarrow 2NO_2$			
*12. $NO + O + M \rightarrow NO_2 + M$	x		x
*13. $NO_2 + O_3 \rightarrow NO_3 + O_2$	x		x
*14. $NO_3 + h\nu$ (red light) → $NO + O_2$	x		x
*15. $NO_2 + NO_3 + M \rightarrow N_2O_5 + M$			
*16. $N_2O_5 + M \rightarrow NO_2 + NO_3 + M$			
*17. $N_2O_5 + h\nu$ (below 380 nm) → $2NO_2 + O$(?)			
*18. $N_2O_5 + O \rightarrow 2NO_2 + O_2$(?)			
*19. $NO_3 + NO \rightarrow 2NO_2$			
*20. $NO_3 + NO_2 \rightarrow NO_2 + O_2 + NO$			
C. Sources and sinks of the active oxides of nitrogen, NO and NO_2			
21. $N_2 + h\nu$ (below 120 nm) → N + N			
*22. $N + O_3 \rightarrow NO + O_2$	x		x
*23. $N + O_2 \rightarrow NO + O$	x		x
*24. $N + NO \rightarrow N_2 + O$	x		x
*25a. $N + NO_2 \rightarrow NO + NO$	x		x
*25b. $N + NO_2 \rightarrow N_2 + O_2$			
*26. $N + OH \rightarrow NO + H$			
27. $N + HO_2 \rightarrow OH + NO$			
*28. $NO + h\nu$ (below 190 nm) → N + O	x		x
Source from troposphere			
29. $N_2O + h\nu \rightarrow N_2 + O(^1D)$	x	x	x
*30. $N_2O + O(^1D) \rightarrow N_2 + O_2$	x		x
*31. $N_2O + O(^1D) \rightarrow NO + NO$	x	x	x
*32. $NH_3 + OH \rightarrow NH_2 + H_2O$			
33. NH_2 + oxides → NO_x(?)			
D. Interactions between odd hydrogen and odd nitrogen			
*34. $HO + NO_2 + M \rightarrow HNO_3 + M$	x	x	x
*35. $HO + HNO_3 \rightarrow H_2O + NO_3$	x		x
*36. $HNO_3 + h\nu$ (below 325 nm) → $HO + NO_2$	x	x	x
*37. $HO + NO + M \rightarrow HNO_2 + M$			
*38. $HO + HNO_2 \rightarrow H_2O + NO_2$			
*39. $HNO_2 + h\nu$ (below 400 nm) → HO + NO			
*40. $N_2O_5 + H_2O$ (on particles) → $2HNO_3$(?)			
*41a. $HO_2 + NO \rightarrow HO + NO_2$	x	x	x
41b. $HO_2 + NO + M \rightarrow HNO_3 + M$(?)			
*42. $HO_2 + NO_2 \rightarrow HNO_2 + O_2$			
E. Reactions of excited oxygen species			
*43a. $O_3 + h\nu$(450-650 nm) → O_2 + O		x	x
*43b. (310-340 nm) → $O_2(^1\Delta) + O(^3P)$	x	x	x
*43c. (below 310 nm) → $O_2(^1\Delta) + O(^1D)$	x	x	x
*43d. (below 220 nm) → O_2 + O(^{1}S) (?)			
*44. $O(^1D) + O_2 \rightarrow O + O_2(^1\Sigma)$			
*45. $O(^1D) + M \rightarrow O + M$	x	x	x
*46. $O_2(^1\Delta) + M \rightarrow O_2 + M$			
*47. $O_2(^1\Sigma) + M \rightarrow O_2 + M$			
48. $O(^1D) \rightarrow O + h\nu$ (630 nm)			
49. $O_2(^1\Sigma) \rightarrow O_2 + hV$ (760 nm)			
50. $O_2(^1\Delta) \rightarrow O_2 + hV$ (1270 nm)			
*51. $O(^1D) + O_3 \rightarrow O_2 + O_2$			
*52. $O_2(^1\Delta) + O_3 \rightarrow O_2 + O_2 + O$			
53. $O_2(^1\Sigma) + O_3 \rightarrow O_2 + O_2 + O$			

	Chang	Prinn	Widhopf
F. Reactions of free radicals based on water (HO_x)			
*54. $O(^1D)+H_2O\rightarrow 2HO$	x	x	x
*55. $O(^1D)+H_2\rightarrow H+HO$	x		
*56. $O(^1D)+CH_4\rightarrow CH_3+HO$	x	x	x
57. $H+O_2+M\rightarrow HOO+M$	x	x	x
*58. $H+O_3\rightarrow HO(v\leq 9)+O_2$	x	x	x
*59. $HO+O\rightarrow H+O_2$	x	x	x
*60. $HO+HO\rightarrow H_2O+O$	x		x
*61. $HO+HO+M\rightarrow H_2O_2+M$			
*62. $HO+HOO\rightarrow H_2O+O_2$	x	x	x
*63. $HOO+HOO\rightarrow H_2O_2+O_2$	x	x	x
*64. $H_2O_2+O\rightarrow HO+HOO$			
*65. $H_2O_2+h\nu\rightarrow HO+HO$	x	x	x
*66. $H_2O_2+HO\rightarrow H_2O+HOO$	x		x
*67. $HO+O_3\rightarrow HOO+O_2$	x	x	x
*68a. $HO(v\geq 2)+O_3\rightarrow H+O_2+O_2$			
*68b. $\rightarrow HOO+O_2$			
*69. $HO(v>3)+O_3\rightarrow OH+O_2+O$			
*70. $HOO+O_3\rightarrow HO+O_2+O_2$	x	x	x
*71. $HOO+O\rightarrow HO+O_2$	x	x	x
*72a. $HOO+H\rightarrow HO+HO$			
*72b. $\rightarrow H_2+O_2$			
*72c. $\rightarrow H_2O+O$			
$H_2O+H\nu\rightarrow H+Oh$		x	
$HO_2+h\nu\rightarrow O+OH$		x	
G. Reactions related to methane			
*73. $O+CH_4\rightarrow CH_3+HO$		x	
*74. $HO+CH_4\rightarrow H_2O+CH_3$			
*75a. $CH_3+O_2\rightarrow CH_3OO$			
*75b. $\rightarrow CH_2O+HO$			
76. $CH_3OO+h\nu\rightarrow H_2CO+HO$ (?)			
*77. $CH_3OO+NO\xrightarrow{h\nu} CH_3O+NO_2$ (?)			
*78. $CH_3OO+NO\xrightarrow{h\nu} CH_3OONO\rightarrow$? (?)			
*79. $CH_3OO+NO_2\rightarrow CH_3OONO_2\rightarrow$? (?)			
*80. $CH_3OO+HO_2\rightarrow CH_3OOH+O_2$			
81. $CH_3O+HO_2\rightarrow CH_3OH+O_2$			
*82. $CH_3O+O_2\rightarrow CH_2O+HO_2$			
83. $CH_3OH+h\nu\rightarrow CH_2O+H_2$ (?)			
84. $CH_3OH+OH\rightarrow H_2O+CH_2OH$			
*85a. $H_2CO+h\nu\rightarrow H_2+CO$			
*85b. $\rightarrow H+HCO$			
*86. $H_2CO+OH\rightarrow HCO+H_2O$			
*87. $H_2CO+O\rightarrow OH+HCO$			
*88. $HCO+O_2\rightarrow CO+HO_2$ (?)			
*89. $OH+H_2\rightarrow H_2O+H$			
*90. $OH+CO\rightarrow CO_2+H$			

[a] The reactions are grouped by reactive species. The notation used is as follows: the underlined reaction number denotes that the reaction is considered to be significant in stratospheric chemistry; the (*) that a summary of available data is available in Ref. 18, and the (?) that the reaction is proposed to explain some effect although it has not been observed in the laboratory. Other reactive species involve sulfur (reactions 91-110) and chlorine (reactions 111-130.)[18]

References

[1] Hidalgo, H., *The Stratosphere, Perturbed by Propulsion Effluents,* U.S. Department of Transportation, Washington, D.C., Appendix E, Summary-CIAP Mon.3,DOT-TST-75-50, Dec. 1974.

[2] Hidalgo, H., *The Natural and Radiatively Perturbed Troposphere,* U.S. Department of Transportation, Washington, D.C., Appendix F, Summary-CIAP Mon. 4, DOT-TST-75-50, Dec. 1974.

[3] *Impacts of Climate Change on the Biosphere,* CIAP Mon. 5, U.S. Department of Transportation, Washington, D.C., in press, 1975.

[4] Venkateswaran, S.V., private communication, Dec. 1974; also Sundararaman, N., St. John, Dennis E., Venkateswaran, S.V., "Solar Ultraviolet Radiation received at the Earth's Surface under Clear and Cloudless Conditions," Department of Meteorology, June 1975, University of California, Los Angeles, Calif.

[5] Herman, B.M. and Browning, S.R., "A Numerical Solution to the Equation of Radiative Transfer," *Journal of Atmospheric Science,* Vol. 22, Sept. 1965, pp. 559-566.

[6] Dave, J.V. and Furukawa, P.M., "Scattered Radiation in the Ozone Absorption Bands at Selected Levels of a Terrestrial, Rayleigh Atmosphere," *Meteorological Monographs,* Vol. 7, American Meteorological Society, Boston, Mass., 1966.

[7] Hunt, G.E., "A Review of Computational Techniques for Analyzing the Transfer of Radiation Through a Model Cloudy Atmosphere," *Journal of Quantitative Spectroscopic Radiation Transfer,* Vol. 11, 1971, pp. 655-690.

[8] Venkateswaran, S.V., et al., *"Radiation in the Natural and Perturbed Troposphere,"* CIAP Monograph 4, in press, 1975.

[9] Dutsch, H.V., "Photochemistry of Atmospheric Ozone," *Advances in Geophysics,* Vol. 15, Academic Press, New York & London, 1971, pp. 219-322.

[10] Leith, C. E., *The Natural and Radiatively Perturbed Troposphere,* CIAP Monograph 4, in press, 1975.

[11] Crutzen, P.J., "Ozone Production Rates in an Oxygen-Hydrogen-Nitrogen Oxide Asmosphere, *Journal of Geophysical Research,* Vol. 76, 1971, pp. 7311-7327.

[12]McElroy, M.B. and McConnell, J.C., "Nitrous Oxide: A Natural Source of Statospheric NO, "*Journal of Atmosphere Science,* Vol. 28, 1971, pp.1095-1098.

[13]Nicolet, M. and Peeterman, W., *Annales Geophysics,* Vol. 28, 1972, p. 751.

[14]Johnston, H.S. and Quitevis, E., "The Oxides of Nitrogen with Respect to Urban Smog, Supersonic Transports, and Global Methane." Presented at *National Congress of Radiation Research,* Seattle, Wash., July 14-20, 1974.

[15]Oort, A.H., and Rasmusson, E.M., "Atmospheric Circulation Statistics," NOAA Prof. Ppr. No. 5, 1971, Geophysical Fluid Dynamics Laboratory, Princeton, N.J.

[16]Lorenz, E.N., "The Nature and Theory of the General Circulation of the Atmosphere, 1967, WMO No. 218, TP. 115, 1967, World Meteorological Organization, Geneva, Switzerland.

[17]Mahlman, J.D., "Preliminary Results from a Three-Dimensional, General Circulation/Tracer Model, DOT-TSC-OST-73-4, *Proceedings of the Second Conference on the Climatic Impact Assessement Program,* Nov. 1972, U.S. Department of Transportation, pp. 321-337.

[18]Johnston, H.S., et al., *Chemistry in the Stratosphere,* CIAP Monograph 1, in press, 1975.

[19]Johnston, H.S., Private Communication, 1973, Dept. of Chemistry, University of California, Berkeley, California.

[20]Mahlman, J.D., "A Three-Dimensional Stratospheric Point-Source Experiment and its Implications for Dispersion of Effluent from a Fleet of supersonic Aircraft," AIAA Paper 73-528, Presented at the AIAA/AMS International Conf. on Enviromental Impacts of Aerospace Operations in the High Atmosphere, Denver, Colo., 1973.

[21]Mahlman, J.D., private communication, Nov. 1974, Geophysical Fluid Dynamics Laboratory, Princeton, New Jersey.

[22]Cunnold, D.M., Alyea, F.N., Phillips, N.A., Prinn, R.G., "First Results of a General Circulation Model Applied to the SST—NO_x Problem," Paper presented at *AIAA Second International Conf. on Environmental Impact of Aerospace Operations in the High Atmosphere,* San Diego, California, July 8-10, 1974.

[23]Dickinson, R., Change, J.S., Geisler, J., Hidalgo, H., Park, J., *Methology for Modeling Global Stratospheric Dynamics and Interactions with Chemical Processes,* CIAP Monograph 3, in press, 1975.

[24]Prinn, R.G., Alyea, F., Katz, A., Cunnold, D., "The Distribution of Odd Nitrogen and Carbon Compounds in the Natural and Perturbed Stratosphere," Paper presented at *AIAA Second International Conf. on Environmental Impact of Aerospace Operations in the High Atmosphere,* San Diego, Calif., July 8-10, 1974.

[25]Gudiksen, P.H., Fairhall, A.W., and Reed, R.J., "Roles of Mean Meridional Circulation and Eddy Diffusion in the Transport of Trace Substance in the Lower Stratosphere, *Journal of Geophysical Research,* Vol. 73, July 1968, pp. 4461-4473.

[26]Widhopf, G.F., "Distribution of Trace Species in the Stratosphere and the Effect of SST Pollutants, presented at *American Geophysical Union,* Fall Annual Meeting, San Francisco, Calif., December 12, 1974.

[27]Danielsen, E.F., et al., *Transport by Mean and Turbulent Motions,* CIAP Monograph 1, in press, 1975.

[28]Cunnold, D.F., Alyea, F., Phillips, N., and Prinn, R., "A Three-Dimensional Dynamical-Chemical Model of Atmospheric Ozone, *Journal of Atmospheric Science,* Vol. 32, Jan. 1975, pp. 170-194.

[29]Cadle, R., et al., *Composition of the Stratosphere,* CIAP Monograph 1, in press, 1975.

[30]Alyea, F.N., Cunnold, D.M., and Prinn, R.G., "Stratospheric Ozone Destruction by Aircraft-Induced Nitrogen Oxides, *Science,* Vol. 188, April 11, 1975, pp. 117-121.

[31]Cunnold, D.M., private commumication , Nov. 1974, MIT Meterology Department, Cambridge, Mass.

[32]*Propulsion Effluents in the Stratosphere,* CIAP Monograph 2, U.S. Department of Transportation, Washington, D.C., in press, 1975.

[33]Robinson, G.D., *The Perturbed Stratosphere—A Summary of Methods Findings,* CIAP Monograph 3, in press, 1975.

[34]Alyea, F.N., et al., *Special Scientific Rept. COO-2294-4,* Sept. 1974, Massachusetts Institute of Technology, Cambridge, Mass.

[35]Crutzen, P.J., "A Review of Upper Atmospheric Photochemistry, *Canadian Journal of Chemistry,* Vol. 52, 1974, pp. 1569-1581.

[36]Crutzen, P.J., "A Two Dimensional Photochemical Model of the Atmosphere Below 55 km. Estimates of Natural and Man-Caused Ozone Perturbations Due to NO_x," National Center for Atmospheric Research, Boulder, Colo., presented at the Fourth Conference on the Climatic Impace Assessment Program, Feb. 1975.